ACS APPLIED MATERIALS & INTERFACES

Research Article

www.acsami.org

Magnetic Nanocomposite Hydrogel for Potential Cartilage Tissue Engineering: Synthesis, Characterization, and Cytocompatibility with Bone Marrow Derived Mesenchymal Stem Cells

Naiyin Zhang,[†] Jaclyn Lock,[†] Amy Sallee,[†] and Huinan Liu*[,†,‡,§]

[†]Department of Bioengineering, University of California, Riverside, California 92521, United States

[‡]Materials Science and Engineering Program, University of California, Riverside, California 92521, United States

[§]Stem Cell Center, University of California, Riverside, California 92521, United States

Supporting Information

ABSTRACT: Hydrogels possess high water content and closely mimic the microenvironment of extracellular matrix. In this study, we created a hybrid hydrogel containing type II collagen, hyaluronic acid (HA), and polyethylene glycol (PEG) and incorporated magnetic nanoparticles into the hybrid hydrogels of type II collagen-HA-PEG to produce a magnetic nanocomposite hydrogel (MagGel) for cartilage tissue engineering. The results showed that both the MagGel and hybrid gel (Gel) were successfully cross-linked and the MagGel responded to an external magnet while maintaining structural integrity. That is, the MagGel could travel to the tissue defect sites in physiological fluids under remote magnetic guidance. The adhesion density of bone marrow derived mesenchymal stem cells (BMSCs) on the MagGel group *in vitro* was similar to the control group and greater than the Gel group. The morphology of BMSCs was normal and consistent in all groups. We also found that BMSCs engulfed magnetic nanoparticles in culture and the presence of magnetic nanoparticles did not affect BMSC adhesion and morphology. We hypothesized that the ingested nanoparticles may be eventually broken down by lysosome and excreted through exocytosis; further studies are necessary to confirm this. This study reports a promising magnetic responsive nanocomposite hydrogel for potential cartilage tissue engineering applications, which should be further studied for its effects on cell functions when combined with electromagnetic stimulation.

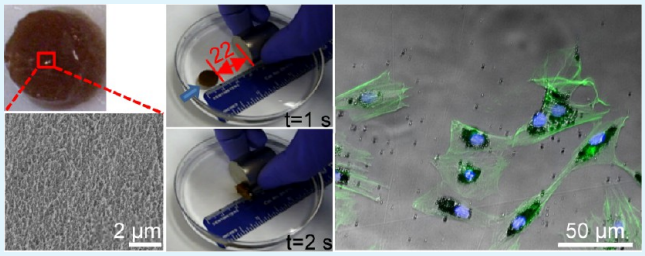

KEYWORDS: *magnetic nanocomposite hydrogel (MagGel), magnetic nanoparticles, hybrid gel, bone marrow derived mesenchymal stem cells, cytocompatibility, cartilage tissue engineering*

1. INTRODUCTION

Currently, natural and synthetic biocomposites, e.g., collagen−PLGA composites,[1] hyaluronic acid−chitosan composites,[2] have been studied for regeneration of cartilage tissue. In addition to the chemistry of the biomaterials, the structure of the scaffold at the nano- and microscale is also vital for cartilage regeneration. Nanomaterials such as nanofibers[3] and materials with nanostructured surfaces[4,5] have been explored to mimic the extracellular matrix (ECM) of cartilage. However, nanostructures developed so far still need further improvement to closely mimic the chemistry and the nano-to-micro structures of native cartilage, induce desirable cellular responses for cartilage regeneration, and provide tunable mechanical properties similar to the ECM.

In recent decades, magnetic nanoparticles have attracted growing interests for biomedical applications. For example, magnetic nanoparticles have been explored extensively as contrast agents to enhance magnetic resonance imaging (MRI) for medical diagnosis,[6] as drug carriers to improve controlled drug delivery to targeted sites,[7] or as hyperthermia agents for cancer treatment.[8] Nevertheless, magnetic nanoparticles alone may not be able to provide optimal properties. Integration of magnetic nanoparticles with other desirable components is an attractive approach to create nanocomposites with integrated properties for biomedical applications. For example, Meenach et al. studied UV-polymerized iron oxide nanoparticles and poly(*N*-isopropylacrylamide) (PNIPAAM) nanocomposites for drug delivery and hyperthermia treatment for cancers; their results showed favorable NIH3T3 murine fibroblasts viability, indicating minimal cytotoxicity.[9] In a few recent studies, magnetic nanoparticles have been incorporated into scaffolds for bone tissue engineering. For instance, Bock et al. transformed standard commercial scaffolds made of hydroxyapatite and collagen into magnetic scaffolds by dip-coating them in aqueous ferrofluids. The results showed that the magnetic nanoparticles were integrated into the porous structures of the scaffolds, and the resulted magnetic scaffolds supported adhesion and proliferation of human bone marrow

Received: July 31, 2015
Accepted: August 28, 2015
Published: September 11, 2015

DOI: 10.1021/acsami.5b06939
ACS Appl. Mater. Interfaces 2015, 7, 20987−20998

derived mesenchymal stem cells (BMSCs) *in vitro*.[10] Zhang et al. developed a three-dimensional magnetic composite scaffold made out of magnetite (Fe_3O_4), mesoporous bioactive glass (MBG), and polycaprolactone (PCL) using a 3D Bioplotter. They reported that the nanocomposite scaffold significantly stimulated human BMSCs proliferation, alkaline phosphatase (ALP) activity, osteogenic gene expression, and ECM mineralization.[11] However, magnetic nanocomposites for soft tissue engineering, e.g., articular cartilage, remains largely unexplored, even though using magnetic nanoparticles or a magnetic field for cartilage tissue engineering showed promising results. Specifically, Kobayashi et al. magnetically labeled human BMSCs using magnetic nanoparticles (ferumoxides) and showed promising results for delivering the cells to degenerated human cartilage to form ECM *in vitro*.[12] Moreover, electromagnetic fields (EMF) have been shown to increase the expression of type II collagen, thus improving chondrogenic differentiation of human BMSCs and stimulating chondrogenesis.[13]

Building on these promising results, we took a new direction of designing magnetic nanocomposite hydrogel scaffolds to harvest the beneficial properties of magnetic nanoparticles while providing a biomimetic, bioactive, and biodegradable platform for potential cartilage tissue engineering. Specifically, we synthesized a novel magnetic nanocomposite hydrogel (MagGel) by mechanical dispersion of magnetic nanoparticles into a hybrid hydrogel (referred to as Gel). The Gel is composed of type II collagen (Col II), hyaluronic acid (HA), and polyethylene glycol (PEG); all these components are biodegradable and provide beneficial properties for cartilage regeneration.

Natural components of Col II and HA are intended to mimic ECM of natural cartilage. Specifically, Col II is the primary protein in hyaline cartilage ECM, where a dense network of fine collagen fibrils provide tensile strength to the tissue.[14] Hyaluronic acid (HA) is a nonsulfated glycosaminoglycan[15] and a major structural component of the ECM in cartilage, which provides compressive strength for cartilage and maintains the ordered structure of collagen.[14,16] HA is known to interact with chondrocyte cell surface receptors such as CD44, which influences endocytosis of HA, and this in turn influences cellular functions.[17] It was reported that the benzyl ester of HA enabled expression of cartilage-specific Col II from chondrocytes, and immobilization of HA onto the surface of poly(D,L-lactic acid-*co*-glycolic acid) scaffolds enhanced adhesion and proliferation of bovine chondrocytes.[18,19] Thus, HA is one of the key factors for cartilage repair due to its ability to support cartilage mechanical strength and influence cellular functions.

The natural polymers of Col II and HA components promote cellular adhesion due to their bioactivity and permit enzymatic degradation, while the multiarmed poly(ethylene glycol) (PEG) component provides the tunable control over physical, chemical, and mechanical properties. PEG is hydrolytically degradable with well documented biocompatibility for cartilage tissue engineering.[20,21] PEG-based hydrogels can be seeded with cells homogeneously and then photopolymerized to form scaffolds *in situ* without damaging living cells.[22] In contrast to natural polymers, PEG alone lacks the biological recognition due to its bioinert nature and thus does not provide an ideal environment for cell adhesion and tissue formation.[23] Copolymerization of PEG with other polymers or monomers can address the inherent limitations of PEG and provide tunable properties. For example, Pfister et al. reported a PEG-dimethacrylate (PEGDMA)-based hydrogel with adjustable shear moduli from 10 kPa to 1 MPa that can mimic mechanical properties of cartilage by altering the PEGDMA concentration.[24] Hutson et al. copolymerized PEG with methacrylated gelatin, and the resulted hydrogel improved fibroblast surface binding when compared with PEG alone.[25] To mimic hyaline cartilage closely, we rationally designed 4-arm-PEG to be copolymerized with Col II and HA, the main proteins in natural cartilage.

The objective of this study was to synthesize a biodegradable and bioactive MagGel scaffold composed of magnetic nanoparticles, Col II, HA, and PEG through chemical cross-linking and mechanical dispersion for potential cartilage tissue engineering applications. We characterized the microstructure and composition of the MagGels, evaluated their magnetic responses and degradation properties in physiological fluids, and investigated their cytocompatibility with BMSCs within 24 h. To our knowledge, this is the first report of designing a bioactive and biodegradable magnetic nanoparticle/organic composite for cartilage tissue engineering. The MagGel developed in this study has a promising potential for cartilage tissue engineering applications.

2. MATERIALS AND METHODS

2.1. Synthesis and Characterization of MagGel. *2.1.1. Synthesis and Characterization of Magnetic Nanoparticles.* Magnetic nanoparticles with poly(vinyl alcohol) (PVA) as the surface modifier were synthesized using the coprecipitation method modified from the procedure reported in the literature.[26] Briefly, PVA (#341584, molecular weight 89 000−98 000, Sigma-Aldrich, St. Louis, MO) was dissolved in deionized water (DI water; Milli-Q Integral Water Purification System, EMD Millipore, Billerica, MA) under the temperature of 100 °C for 30 min to make 50 mg/mL PVA solution. $FeCl_3$ (#169430010, Sigma-Aldrich, St. Louis, MO) and $FeCl_2{\cdot}4H_2O$ (#44939, Sigma-Aldrich, St. Louis, MO) powder with a molar ratio of 2:1 was then dissolved in the 50 mg/mL PVA solution and stirred at room temperature for an additional 30 min. A 25-gauge needle was used to gradually drop the aqueous mixture of PVA/$FeCl_3$/$FeCl_2{\cdot}4H_2O$ into 15 mL of 10%-diluted ammonium hydroxide solution (#338818, Sigma-Aldrich, St. Louis, MO) to produce magnetic nanoparticles. The magnetic nanoparticles were washed with DI water for three times, dried overnight, and ground using a mortar and pestle.

The surface morphology and elemental composition of the magnetic nanoparticles (MNPs) were examined using a scanning electron microscope (SEM; Nova NanoSEM450, FEI) and the attached detector for energy dispersive X-ray spectroscopy (EDS; X-Max 50 silicon drift detector), respectively. The magnetic nanoparticles were mounted onto the SEM sample holder using the copper tape. An acceleration voltage of 10 kV and Everhart-Thornley secondary electron detector was used for SEM imaging, and an acceleration voltage of 20 kV and EDS detector was used for elemental composition analysis. The size of nanoparticles was analyzed on the basis of the high-resolution SEM image using the quantitative analysis tools of ImageJ software. The Feret diameter of 200 magnetic nanoparticles was measured using ImageJ, and the average Feret diameter was calculated with an assumption that the synthesized MNPs are spherical. Alternatively, the size and distribution of magnetic nanoparticles were analyzed using a laser diffraction-based technique (Beckman Coulter LS 13 320 Particle Size Analyzer, Beckman Coulter, Inc., Brea, CA). Briefly, a suspension with 10 mg/mL of magnetic nanoparticles was prepared by dispersing magnetic nanoparticles into DI water; the suspension was then added into the universal liquid module of the Beckman Coulter particle size analyzer, further sonicated to improve dispersion, and analyzed using laser diffraction. The crystal structure of the magnetic nanoparticles was

DOI: 10.1021/acsami.5b06939
ACS Appl. Mater. Interfaces 2015, 7, 20987−20998

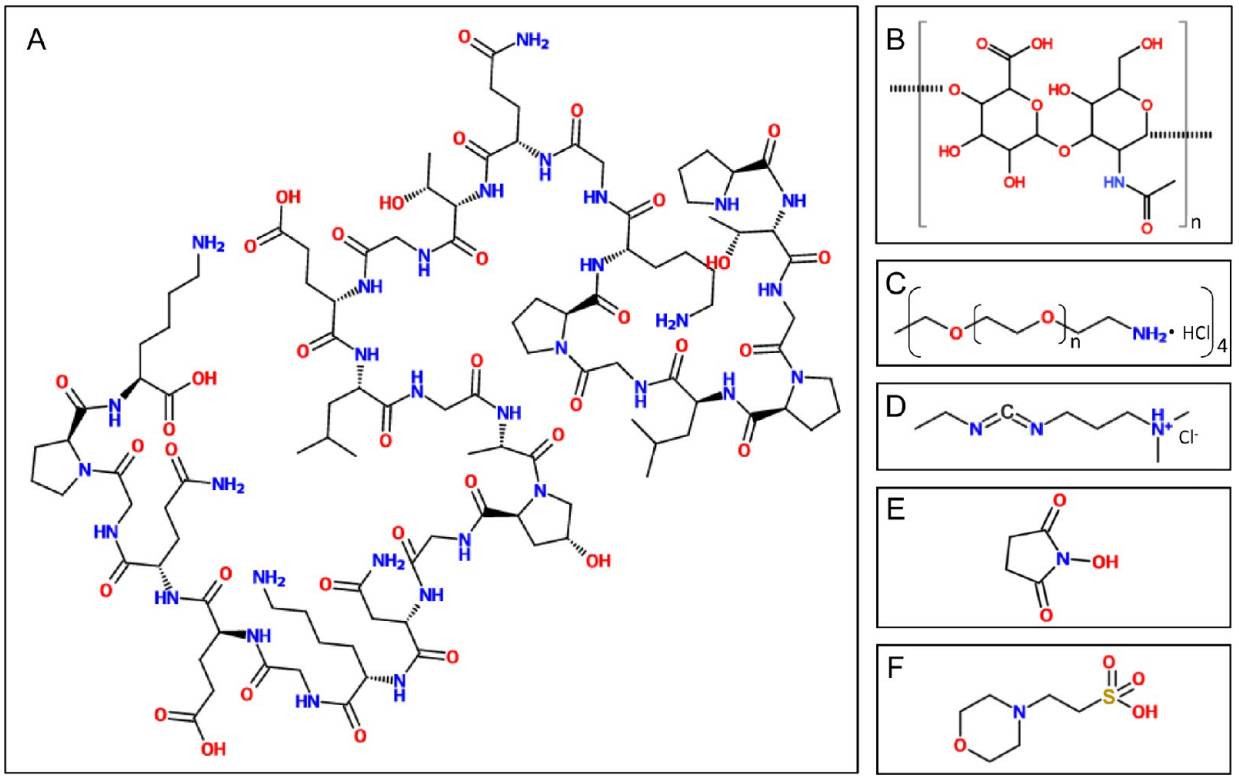

Figure 1. Chemical structures of each component used for synthesizing the magnetic nanocomposite hydrogels (MagGel) and the hybrid hydrogels (Gel). (A) Representative type II collagen fragment (CAS No. 144703-90-2), (B) HA, (C) 4-arm-PEG, (D) EDC·HCl, (E) NHS, and (F) MES buffer.

analyzed using X-ray diffraction (XRD; PANalytical X-ray diffractometer, Empyrean) at 45 kV and 40 mA with a 0.02° step size.

2.1.2. Extraction and Characterization of Cartilage and Collagen. Subchondral bone plugs with hyaline cartilage (0.5 cm in diameter) were harvested from the stifle joints of two-year-old sheep using an osteochondral autograft transfer system (Arthrex OATS, Arthrex, Inc., Naples, FL). The bone plug was photographed using a camera (Coolpix L22 12.0 MP, Nikon, Japan). The bone plug was then prepared for SEM imaging through rapid freezing in liquid nitrogen. The surface and cross-section of the bone plug was examined using an environmental SEM (Hitachi TM-1000 Tabletop Scanning Electron Microscope, Hitachi High-Technologies America, Inc.).

Type II collagen (Col II) was extracted from the harvested cartilage following a protocol modified from the procedure reported in the literature.[27] Briefly, stifle joints of two-year-old sheep were harvested and dissected to expose articular cartilage. The articular cartilage surface was rinsed with 70% isopropyl alcohol (#I9030, Sigma-Aldrich, St. Louis, MO) followed by phosphate buffered saline (PBS; #2810305, MP Biomedicals, LLC, Solon, OH). A scalpel was used to scrape the articular cartilage from the femoral condyle, tibia plateau, and patella. The cartilage pieces were minced in ice-cold 0.025 M Tris(hydroxymethyl) aminomethane (Tris buffer, #252859, Thermo Fisher Scientific, Inc., Waltham, MA) to improve Col II extraction. The cartilage was mixed on a rotator (#11-402-12, Fisher Scientific, Waltham, MA) overnight in a solution of 2.5 M guanidine (#BP178-500, Thermo Fisher Scientific, Inc., Waltham, MA) in 0.025 M Tris buffer at 4 °C. The cartilage was washed three times with cold DI water for 30 min at 4600*g* and 4 °C to remove guanidine. The supernatant was removed, and the cartilage was resuspended in 500 mM acetic acid (#320099, Sigma-Aldrich, St. Louis, MO) and adjusted to pH 2.8. Next, 1 g of pepsin (#P7000, Sigma-Aldrich, St. Louis, MO) was added for every 20 g of cartilage, and the suspension was mixed for 48 h at 4 °C. The suspension was centrifuged for 30 min at 5000*g* at 4 °C, and the supernatant was collected. Then, 5 M NaCl (#S3014, Sigma-Aldrich, St. Louis, MO) was added to a final concentration of 0.8 M, and collagen was allowed to precipitate for 24 h. The precipitated collagen was collected by centrifuging at 4600*g* for 60 min at 4 °C and resuspended in 100 mM acetic acid overnight at 4 °C. The collagen solution was dialyzed against PBS overnight at 4 °C. The extracted collagen was lyophilized and stored at −20 °C until use.

Extracted type II collagen was characterized using Fourier Transform Infrared Spectroscopy (FTIR, Nicolet 6700 FTIR spectrometer, Thermo Fisher Scientific Inc., Waltham, MA). Briefly, potassium hydroxide (KOH) was heated overnight to remove residual water. The mixture of collagen and KOH was ground using a mortar and pestle and pressed into a pellet at 10 000 psi. The translucent pellet was placed in the FTIR sample holder and scanned at the wavenumbers between 4000 and 500 cm^{-1}.

2.1.3. Synthesis of the MagGel and Gel. The hybrid gel (Gel) was synthesized through chemical cross-linking, modified from the process reported by Calderon et al.[28] Figure 1 shows the chemical structures of the representative Col II fragment and other major components used in the Gel synthesis. Briefly, 1-ethyl-3-(3-(dimethylamino)propyl)-carbodiimide·HCl (EDC·HCl, hereafter referred as EDC, #22980, Thermo Fisher Scientific Inc., Waltham, MA) was dissolved in 2-(*N*-morpholino)ethanesulfonic acid (MES buffer, #28390, Thermo Fisher Scientific Inc., Waltham, MA) by vortex to obtain a concentration of 19 mg/mL as the cross-linking reagent. HA (#HA200 K-1, Lifecore Biomedical, LLC, Chaska, MN) and Col II (extracted from sheep femur condyle and tibia plateau) were added into EDC solution followed by the addition of extra MES buffer to help dissolve HA and Col II. Col II and HA had a weight ratio of 9:1 to mimic cartilage ECM. Afterward, 4-arm-PEG (#4arm-NH2-10K, JenKem Technology, Allen, TX) was added to achieve the Col II/HA/PEG weight ratio of 9:1:2 and mixed by vortex and sonication. The mixture was then divided into two separate microcentrifuge tubes; magnetic nanoparticles were added into one tube to produce the MagGel (A), while the other tube was left alone for the formation of the Gel (B). Additional MES buffer was added into each tube and sonicated to help dissolve 4-arm-PEG. In the (A) MagGel, the dry weight ratio of magnetic nanoparticles to the Col II/HA/PEG gel was 1:24. *N*-Hydroxysuccinimide (NHS, #24500, Thermo Fisher Scientific Inc.,

DOI: 10.1021/acsami.5b06939
ACS Appl. Mater. Interfaces 2015, 7, 20987−20998

Waltham, MA) was dissolved in MES buffer and added to A and B, respectively, to induce further cross-linking and produce stable Col II/HA/PEG hydrogel with or without magnetic nanoparticles. A and B solution were then transferred into the wells of a 48-well plate and incubated at 37 °C for 24 h. Afterward, additional EDC was added to each solution and incubated in a 37 °C incubator overnight to further cross-link Col II, HA, and 4-arm-PEG. The resulted MagGel and Gel samples had a similar dimension and volume to be consistent for *in vitro* degradation and cell study.

2.1.4. Characterization of the MagGel in Comparison with the Gel. The MagGel and Gel were dehydrated in a series of ethanol solutions with concentrations of 30%, 50%, 70%, 80% 90%, 95%, and finally 100%, 1 h in each concentration of ethanol. The dehydration in 100% ethanol was repeated three times. The samples were then transferred to a 50 mL conical tube with the tube screwed lightly onto the cap and kept inverted. The inverted tube was dipped into liquid nitrogen for 30 s. After that, the samples were kept in the cap of the conical tube and covered with Parafilm M (#PM992, Bemis Flexible Packaging, Neenah, WI) with a few punctures generated by a 25 G needle. The covered cap was loaded into a freeze-dry-system (cat# 7934026, FreeZone Plus 6 Cascade Console Freeze-Dry System, Labconco, Kansas City, MO) and left overnight. The freeze-dried sample was characterized using FTIR (Nicolet 6700 FTIR spectrometer, Thermo Fisher Scientific Inc.). The microstructure of the lyophilized samples was observed using SEM, and the elemental composition was quantified using energy dispersive X-ray spectroscopy (EDS; AZtec, Oxford instruments).

2.2. Magnetic Response of the MagGel and Magnetic Nanoparticles. The response of the MagGel and magnetic nanoparticles to the external magnetic field was tested using a N42 neodymium magnet (#DEX0, K&J Magnetics, Inc., Pipersville, PA) with a diameter of 22 mm and a height of 25 mm. MagGel with a diameter of 11 mm and a height of 3 mm was immersed in a Petri dish filled with MES buffer, and the neodymium magnet was placed 3 cm away from the right side of the hydrogel. The magnet was slowly moved toward the hydrogel, and magnetic response was recorded. To study remote magnetic guidance, MagGel was immersed in a Petri dish filled with MES buffer, and the neodymium magnet was applied above the dish to direct the MagGel to move from one side of the dish to the other side. The diameter of the dish was 8 cm, and the movement of the MagGel guided by the external magnet was recorded. The vertical and horizontal movement of MagGel in response to the magnet was tested in a 15 mL centrifuge tube filled with MES buffer. In the vertical movement test, after the MagGel settled to the bottom of the centrifuge tube by gravity, the magnet was placed outside the tube and moved up against gravity. For the horizontal test, the centrifuge tube was placed horizontally and the magnet was applied on the side of the tube to direct the MagGel to move horizontally from one end to the other end of the tube. The whole process of vertical and horizontal movement was recorded. In addition, the response of magnetic nanoparticles to the magnet was recorded separately. A small amount of magnetic nanoparticles weighing 1 mg was mechanically dispersed in 1 mL of DI water using vortex. The magnet was placed about 5 mm away from the microcentrifuge tube, and the time needed to collect the dispersed magnetic nanoparticles toward the magnet was recorded. Please see Supplemental Videos 1 and 2 for these experiments on magnetic responses.

2.3. Degradation Study of the MagGel versus Gel. The MagGel was stored in MES buffer before the degradation study in the revised simulated body fluid (rSBF). The rSBF had the same ionic concentration as human blood plasma, containing Na^+ (142.0 mM), K^+ (5.0 mM), Mg^{2+} (1.5 mM), Ca^{2+} (2.5 mM), Cl^- (103 mM), HCO_3^- (27 mM), HPO_4^{2-} (1.0 mM), and SO_4^{2-} (0.5 mM) ions. MES buffer was removed at the beginning of the degradation study, and 5 mL of rSBF was added to the Petri dish to submerge the MagGel sample. The samples were incubated in an incubator at 37 °C, and 1 mL of rSBF was added to the Petri dish every day to compensate the fluid loss due to evaporation. The lyophilized Gel was incubated in a phosphate buffered saline (PBS) following a similar procedure. PBS was composed of 137 mM sodium chloride, 2.68 mM potassium chloride, 1.47 mM KH_2PO_4, and 8.1 mM Na_2HPO_4, with corresponding ions of Na^+ (153.2 mM), K^+ (4.2 mM), Cl^- (139.7 mM), HPO_4^{2-} (8.1 mM), and $H_2PO_4^-$ (1.5 mM). The testing samples were weighed every day until they lost structural integrity.

2.4. *In Vitro* Cytocompatibility Study with BMSCs. *2.4.1. Preparation of BMSC Culture.* Dulbecco's modified Eagle's medium powder (DMEM, #SLBC9050, high glucose, D5648, Sigma-Aldrich, St. Louis, MO) and sodium bicarbonate ($NaHCO_3$; #S5761, Sigma-Aldrich, St. Louis, MO) were dissolved in DI water to obtain a media with DMEM and $NaHCO_3$ concentration of 13.4 and 3.7 mg/mL, respectively. The pH of media was adjusted to 7.1 by adding 1 M hydrogen chloride (HCl) solution. The media were sterilized using a 0.2 μm filter (#596-0020, Thermo Fisher Scientific, Inc., Waltham, MA). For BMSC culture, the media were supplemented with 10% fetal bovine serum (FBS; HyClone, #SH30910, Thermo Fisher Scientific Inc., Waltham, MA) and 1% penicillin/streptomycin (P/S; HyClone, #SV30010, Thermo Fisher Scientific, Inc., Waltham, MA). Hereafter, DMEM + $NaHCO_3$ + 10% FBS + 1% P/S is referred to as DMEM.

BMSCs were harvested from the marrow cavity of the femur and tibia of 3-week-old Sprague−Dawley rat weanlings immediately after euthanasia by CO_2 asphyxiation. The protocol for harvesting BMSCs was approved by the Institutional Animal Care and Use Committee (IACUC) at the University of California at Riverside and established previously in our laboratory.[29] Briefly, the distal and proximal ends of the harvested femur and tibia were dissected, and the bone marrow was flushed out of the marrow cavity and collected using DMEM. The collected bone marrow was filtered through a 70 μm nylon strainer (#22363548, Thermo Fisher Scientific, Inc., Waltham, MA) to remove cell aggregates and tissue debris. The filtered cells were cultured in DMEM under standard cell culture conditions (i.e., 37 °C, 5% CO_2/95% air, humidified, sterile environment) to 90−95% confluency prior to the *in vitro* study with the materials of interest.

2.4.2. Sample Preparation for Cell Culture. MagGel and Gel samples were cut into quarters for BMSC study. Three pieces of MagGel and three pieces of Gel were sterilized by soaking in 70% ethanol solution for 20 min. Magnetic nanoparticles were placed in a microcentrifuge tube and exposed to ultraviolet radiation for 2 h to disinfect. Glass slides with a dimension of 1 cm × 1 cm were cut from Fisher premium microscope slides (#12-544-1, Thermo Fisher Scientific, Inc., Waltham, MA). Six glass slides were cleaned with acetone and 70% ethanol solution using a bath sonicator for 1 h each and then exposed to ultraviolet radiation for 2 h to disinfect. Three glass slides were used as substrates to support magnetic nanoparticles; magnetic nanoparticles on glass slides were used as the particle control. The other three glass slides were used as a reference group for BMSC culture.

After sterilization, three pieces of MagGel, three pieces of Gel, and six pieces of glass slides were placed into separate wells of a 12-well tissue culture-treated plate. MagGel and Gel samples were placed directly into the culture well without the glass slides. Magnetic nanoparticles of 2.5 mg were suspended in 40 μL of DMEM homogeneously. Each 10 μL of the magnetic nanoparticle suspension was gently pipetted onto each of the three glass slides. The mass of magnetic nanoparticles in each well was the same as that in each piece of MagGel. Each well was gently rinsed with 2 mL of PBS to equilibrate the well and samples before seeding cells. The neodymium magnet was used to prevent aspiration of magnetic nanoparticles during rinsing steps.

2.4.3. BMSC Culture with the Samples. BMSCs were washed with PBS and detached from the culture flasks using trypsin (#25200-056, Life Technologies, Carlsbad, CA). BMSCs in each flask were collected into a 15 mL-centrifuge tube and centrifuged for 5 min at 1000 rpm. After the supernatant was removed, the BMSCs were resuspended in fresh media. Cell suspension was mixed with trypan blue solution (#T8154, Sigma-Aldrich, St. Louis, MO) at a dilution factor of 2, and the cell number was counted using a hemocytometer (#1475, Reichert Bright-Line, Hausser Scientific, Horsham, PA). The volume of cell suspension needed for seeding at a density of 10 000 cells/cm^2 was calculated on the basis of the cell count. BMSCs were diluted to the needed concentration using fresh DMEM, and then, 2 mL of the

DOI: 10.1021/acsami.5b06939
ACS Appl. Mater. Interfaces 2015, 7, 20987−20998

diluted cell suspension was pipetted into each well of the 12-well plate for the culture of cells on the surface of the gels. The culture plate was gently placed back into the incubator and cultured for 24 h under the standard cell culture conditions.

2.4.4. Characterization of BMSC Adhesion and Morphology. After 24 h, the media were collected from each well and the samples were moved to a new 12-well plate. Nonadherent cells were washed away using PBS. Adhered cells on the 12-well plate or on the samples were fixed with 4% paraformaldehyde (PFA; #15714-S, Electron Microscopy Science, Hatfield, PA) solution, stained with Alexa Fluor 488 Phalloidin (#A12379, Life Technologies, Carlsbad, CA) for F-actin and 4′,6-diamidino-2-phenylindole (DAPI; #D3571, Life Technologies, Carlsbad, CA) for cell nuclei. After fixing and staining, cells were imaged using a fluorescence microscope (Nikon T*i*-S eclipse, Nikon, Japan), and the images were merged using ImageJ. Cell adhesion density (cells/cm^2) was calculated for each sample. Briefly, five random spots in each well were imaged, and the number of cells in each image was quantified. The cell density in each image area (or spot) was calculated using eq 1, and the average cell density in each well was calculated using eq 2.

$$\text{cell density in spot } i = \frac{\text{cell number in image } i}{\text{area of image } i} \quad (1)$$

in which i represents the random imaging spot from 1 to 5 in each well. Image area is in the unit of cm^2.

$$\text{average cell density} = \frac{\sum_1^i \text{cell density in spot } i}{5} \quad (2)$$

2.5. Statistical Analysis. Experiments were run in triplicate, and the data were analyzed using one-way analysis of variance (ANOVA) followed by the Tukey's Honest Significant Difference (HSD) posthoc test. Statistically significant difference was considered at $p < 0.05$.

3. RESULTS

3.1. Characterization of Materials of Interest. *3.1.1. Characterization of Magnetic Nanoparticles.* The synthesized magnetic nanoparticles exhibited spherical morphology, as shown in the scanning electron micrograph at a high magnification of 100 000× (Figure 2A). The corresponding EDS analyses (Figure 2B) showed the presence of iron (Fe; 24 at. %), oxygen (O; 49 at. %), carbon (C; 26 at. %) and a trace amount of chlorine (Cl; 1%). As expected, C was detected due to the PVA surface modifier. The trace Cl might be a result of residual reactant that was not completely washed away after the synthesis; more thorough washes will be helpful in the future research. Quantitative analysis of the SEM image of nanoparticles showed that the average diameter of the magnetic nanoparticles was 15 ± 5 nm (Figure 2C), while the particle analysis result from laser diffraction indicated the average diameter of magnetic particles to be 77 ± 4 nm (Figure 2D). This difference observed was most likely due to nanoparticle agglomeration during laser diffraction measurement. XRD pattern confirmed that the synthesized nanoparticles were iron oxide (Figure 2E). The major XRD peaks for Fe_3O_4 and γ-Fe_2O_3 are very close to one another according to the standard XRD pattern (PDF #19629 and #39-1346, respectively). As shown in Figure 2E, major peaks for Fe_3O_4 were present, and the minor peaks for γ-Fe_2O_3 were absent, indicating the synthesized nanoparticles were most likely to be in the Fe_3O_4 phase.

3.1.2. Characterization of Articular Cartilage and Extracted Collagen. The surface and cross-section of the dissected bone plug were characterized using SEM (Figure 3). Figure 3A showed the sheep femur condyle where the bone plugs were harvested. Figure 3B showed the side of the bone

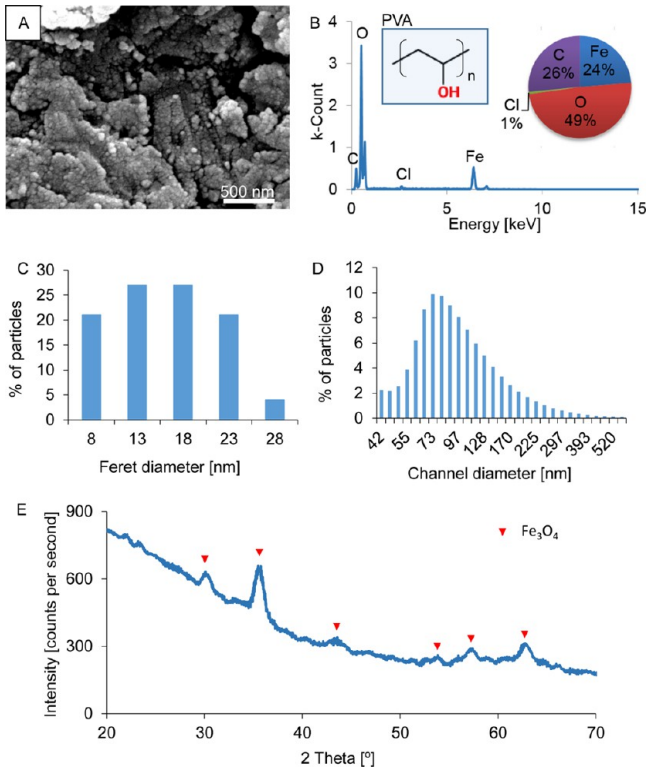

Figure 2. Characterization of magnetic nanoparticles. (A) SEM image. Scale bar = 500 nm. Original magnification = 100 000×. (B) EDS spectrum and quantification of elemental composition of magnetic nanoparticles in atomic percent (at. %). Inset: chemical structure of PVA. (C) Particle size and distribution based on quantitative analysis of SEM image in (A) using ImageJ software. (D) Particle size and distribution analyzed using laser diffraction. (E) XRD spectrum of magnetic nanoparticles.

plug used for SEM characterization. Figure 3C showed the overview of the zonal transition in the bone plug from the articular surface to mineralized subchondral bone. Figure 3C1−C6 provided a magnified view for each transition area between the articular cartilage to subchondral bone. Figure 3C1 showed the smooth surface of articular cartilage. Figure 3C2−C4 showed the microstructural changes in collagen network as we gradually moved the area of observation from articular cartilage surface to subchondral bone. Figure 3C5,C6 showed increasing particulate mineral content toward the cartilage−bone interface, correlated to the changes in mechanical properties between cartilage and bone.

Type II collagen extracted from the sheep femur condyle or tibia plateau was characterized using FTIR, as shown in Figure 4. The FTIR spectrum for type II collagen from femur condyle cartilage showed clear peaks for amide A, I, II, and III at 3420, 1653, 1560, and 1229 cm^{-1}, respectively (Figure 4A). Amide A band is due to the N−H stretching vibration in protein backbone, and amide I is the most intense absorption band in protein that is primarily dominated by the stretching vibrations of the C═O and C−N groups. The amide II and amide III bands are largely dependent on the N−H bending vibrations in protein. In comparison with the collagen from femur condyle cartilage, the collagen from tibia plateau cartilage showed a clear presence of amide A and I peaks at 3435 and 1661 cm^{-1}, respectively, but the peaks for amide II and III groups are smaller at 1559 and 1235 cm^{-1}, respectively (Figure 4A′).

DOI: 10.1021/acsami.5b06939
ACS Appl. Mater. Interfaces 2015, 7, 20987−20998

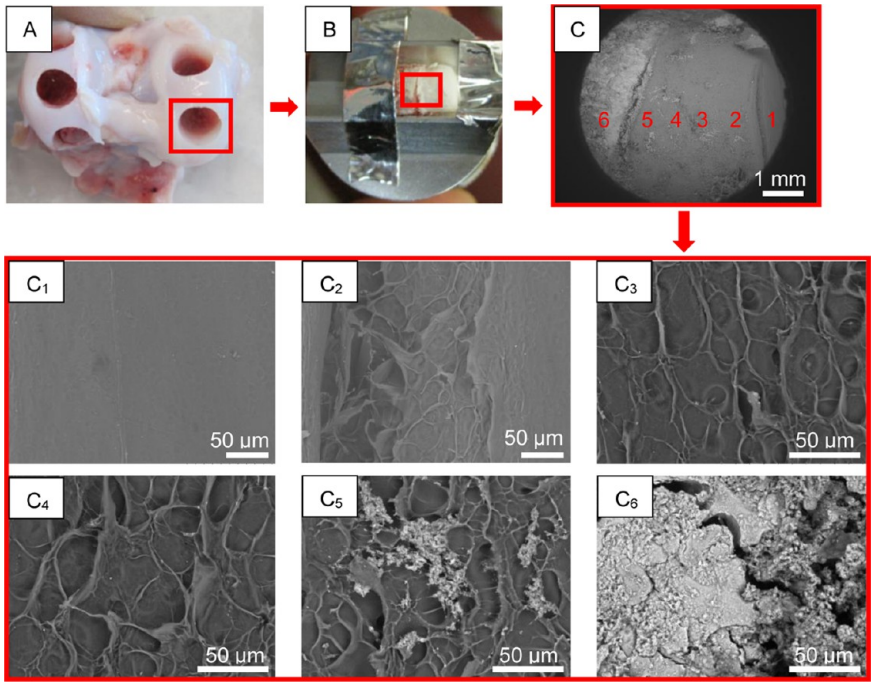

Figure 3. Characterization of cartilage tissue harvested from sheep femur condyle. (A) Photograph of sheep femur condyle where bone plugs were harvested. (B) Photograph of a harvested bone plug. (C) SEM image of the bone plug cross-section from articular surface to subchondral bone at low magnification. (C_1–C_6) Magnified SEM images of the transition area from articular surface to subchondral bone. Original magnification for C_1 and C_2 is 600×, and for C3-C6, it is 1000×. Scale bar = 50 μm.

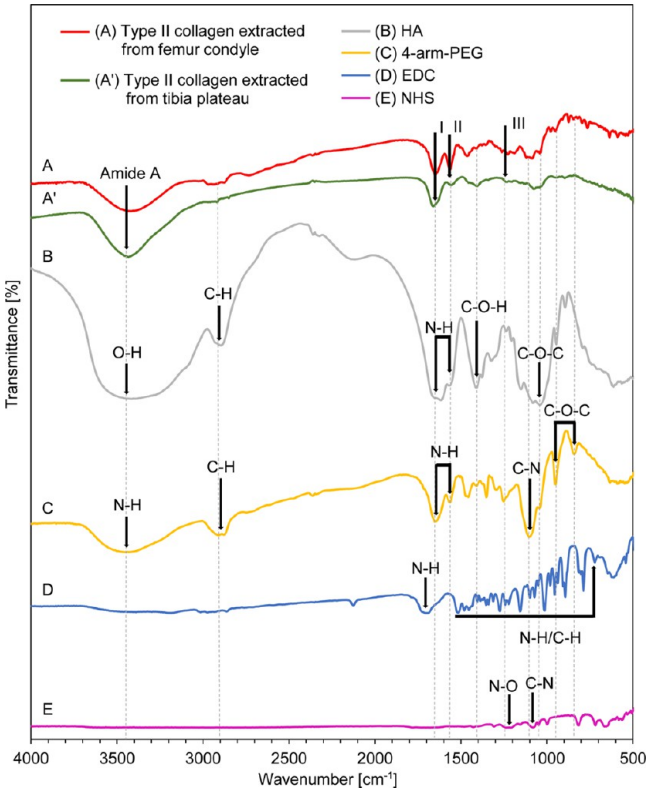

Figure 4. FTIR spectra of type II collagen extracted from sheep femur condyle or tibia plateau, and HA, 4-arm-PEG, EDC, and NHS used for the synthesis of MagGel and Gel. (A) Type II collagen extracted from femur condyle, (A′) type II collagen extracted from tibia plateau, (B) HA, (C) 4-arm-PEG, (D) EDC, and (E) NHS.

Generally, the collagen from cartilage tissues at femur condyle or tibia plateau showed similar spectra.

The components for hydrogel synthesis, including HA, PEG, EDC, and NHS, were also characterized using FTIR. The broad peak centered around 3450 cm^{-1} is typical for O−H stretching vibration of HA and N−H stretching vibration of 4-arm-PEG. The relatively narrower peaks at 2897 cm^{-1} resulted from C−H stretching vibration of both HA and 4-arm-PEG. The small peaks shown on HA spectrum at 1616 and 1566 cm^{-1} can be assigned to N−H bending, and the two peaks at 1410 and 1044 cm^{-1} are due to C−O−H stretching and C−O−C stretching vibrations, respectively.[30] The two adjacent peaks at 1650 and 1570 cm^{-1} are due to the N−H stretching vibration in the 4-arm-PEG. The narrow peak on 4-arm-PEG spectrum at 1111 cm^{-1} can be assigned to the C−N stretching vibration, and the two small peaks at 951 and 843 cm^{-1} can be assigned to C−O−C asymmetric stretching vibration.[31] The first broadest peak at 1705 cm^{-1} on the EDC spectrum shows the N−H bending vibration, and the following region of multiple peaks from 1500 to 700 cm^{-1} can be assigned to C−N stretching or N−H bending vibrations.[32,33] Compared with other components, the peaks on the FTIR spectrum of NHS are relatively smaller but still recognizable. The peak at 1213 cm^{-1} shows the N−O stretching vibration in NHS,[34] and the peak at 1084 cm^{-1} represents the C−N stretching vibration.

3.1.3. Characterization of the MagGel in Comparison with the Gel. FTIR spectrum of MagGel was compared with that of the Gel in Figure 5. The FTIR spectra indicated that Type II collagen was incorporated since the peaks for amide A, I, II, and III were present, and the peak intensities of MagGel are greater than that of Gel. Significant differences in the FTIR spectra at wavenumber 945.8 and 842.7 cm^{-1} for the MagGel and Gel were observed; these peaks are due to C−O−C stretching and N−H bending vibrations, respectively. SEM images and EDS

DOI: 10.1021/acsami.5b06939
ACS Appl. Mater. Interfaces 2015, 7, 20987−20998

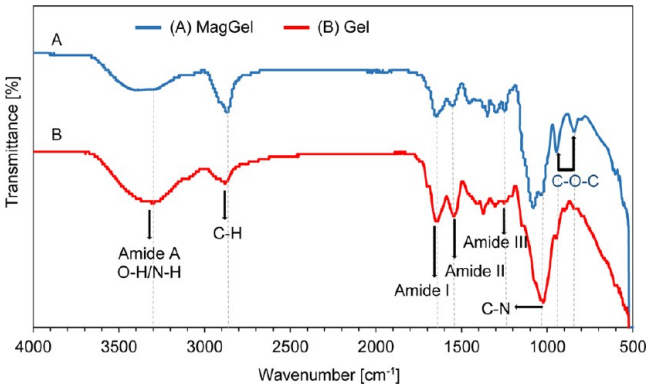

Figure 5. FTIR spectra of (A) MagGel and (B) Gel.

analyses of the lyophilized MagGel and Gel are shown in Figure 6. Both types of gels showed micron-scale porous structures,

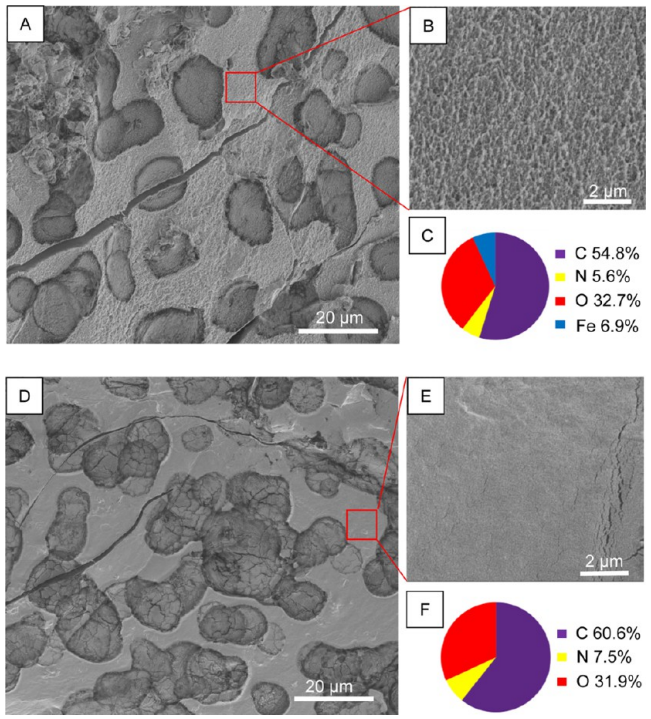

Figure 6. SEM images and EDS quantitative analysis (at. %) of (A–C) MagGel and (D–F) Gel. (A, D) Low magnification SEM images; original magnification = 1000×. (B, E) High magnification SEM images; original magnification = 10 000×. (C, F) EDS elemental analysis of (A) MagGel and (D) Gel, performed at 1000×.

and the MagGel showed a rougher surface when compared with the Gel at a higher magnification of 10 000× (Figure 6A,B,D,E). The EDS analyses confirmed that the lyophilized MagGel contained C, N, O, and Fe (Figure 6C), while the Gel contained C, N, and O (Figure 6F). The gels were sputter coated with Pt/Pd prior to SEM and EDS analyses, which was excluded in quantification of elemental compositions.

3.2. Magnetic Responses in Aqueous Solutions. The MagGel showed magnetic response when exposed to an external magnet (Figure 7A). When the magnet was placed more than 22 mm away from the MagGel, there was no response. When the distance was reduced to 22 mm, the MagGel moved to the magnet in 1 s. In another test (see Supplemental Video 1), the diameter of the dish was 8 cm and the time for the MagGel to travel across this 8 cm distance was 3 s, so the approximate speed of the gel movement in MES buffer was 26.7 mm/s. The speed of the gel movement may be fine-tuned by adjusting the moving speed of the magnet and its magnetic intensity. The vertical movement test showed that the MagGel can be moved against gravity. The MagGel and magnet both had a cylindrical shape. Thus, the geometric center of the top or bottom cross section of MagGel had the strongest magnetic interactions with the top or bottom of the magnet, when compared with side-to-side magnetic interactions between the MagGel and the magnet. The horizontal movement of the same MagGel in the same centrifuge tube further confirmed this.

Figure 7B shows the response of magnetic nanoparticles to the same external magnet when suspended in DI water. When exposed to the magnet, the nanoparticles were attracted to the side of magnet placed 5 mm away within 3 s (Supplemental Video 2).

3.3. Degradation of the MagGel and Gel in Aqueous Solutions at 37 °C. Both MagGel and Gel absorbed water and swelled when they were cultured in SBF or PBS, as shown in Figure 8. Figure 8A shows the photographs of MagGel during the 21-day degradation study in SBF, and Figure 8B shows the degradation of Gel in PBS. Both the MagGel and Gel lost structure integrity after 21 days of immersion in aqueous solutions at 37 °C. The surface morphology of both MagGel and Gel changed over time during degradation. The mass change over time confirmed water absorption during immersion in physiologically relevant fluids. Specifically, for MagGel, the initial wet mass was 400.2 mg and increased to 1402.2 mg on day 21, which was 3.5-fold of the initial mass. As for the Gel, after immersion, it became too soft to be picked up for the weight measurement without damaging the structure.

3.4. BMSC Adhesion and Morphology when Cultured with the MagGel, Gel, and Magnetic Nanoparticles. Figure 9 shows the adhesion and morphology of BMSCs after being cultured with MagGel, Gel, magnetic nanoparticles on glass slides, and a glass reference for 24 h. The BMSCs that adhered on the culture well with each sample were imaged. Surprisingly, both the MagGel and Gel samples lost structural integrity in BMSC culture and became visually undetectable in the culture wells after 24 h. Thus, BMSCs could not be imaged on the samples. Interestingly, BMSCs engulfed nanoparticles and retained viability, as shown in Figure 9E,F. These magnetic nanoparticles appeared to be within the cytoplasm of the cells and close to the nuclei, but not in the cell nuclei. Some magnetic nanoparticles were also found to be outside of the cells. BMSC adhesion density in each well was quantified, as shown in Figure 10. Among all the groups, MagGel showed the highest average cell density, similar to the glass reference, but no statistically significant difference was detected. The Gel group showed the least cell density on average, less than the magnetic nanoparticle group, but no statistically significant difference was detected. The ANOVA analysis showed that there was no statistically significant difference among all the groups ($p = 0.0563 > 0.05$).

4. DISCUSSION

4.1. Characterization of Magnetic Nanoparticles. The magnetic nanoparticle size was 15 ± 5 nm, as characterized by SEM (Figure 2A,C). The nanoparticles were attracted to the external magnet (Figure 7B), indicating their paramagnetic

DOI: 10.1021/acsami.5b06939
ACS Appl. Mater. Interfaces 2015, 7, 20987–20998

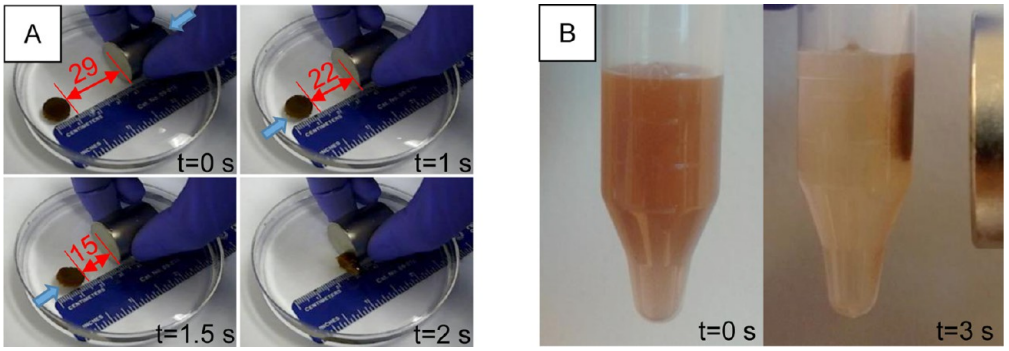

Figure 7. Magnetic responses of the synthesized MagGel and magnetic nanoparticles to a magnet. (A) MagGel in MES buffer (unit of numbers in red: mm) and (B) magnetic nanoparticles in DI water. Blue arrows indicate the object movement direction before the next time point. Details are available in the Supplemental Videos 1 and 2.

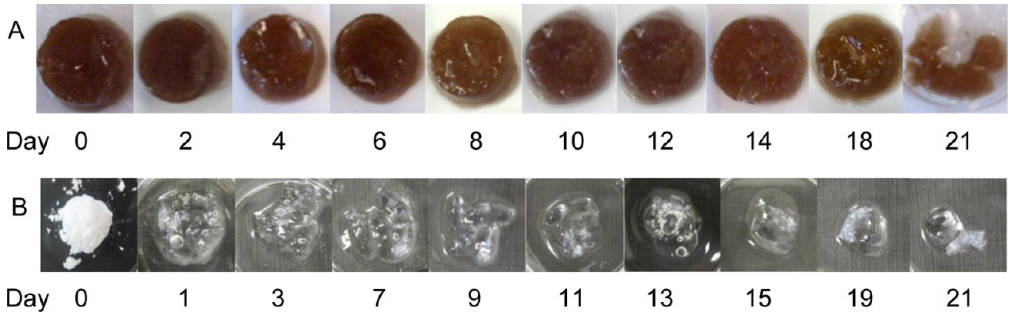

Figure 8. Macroscopic photographs of materials of interest during 21 days of degradation at 37 °C. (A) MagGel degradation in rSBF and (B) Gel degradation in PBS.

property. Paramagnetic property enables magnetic moments inside the magnetic nanoparticles to align in the same direction as the external magnetic field, and the nanoparticles would not retain any remnant magnetization upon removal of the external magnetic field. Paramagnetic property enabled magnetic nanoparticles to become dispersed again after removal of the magnetic field, which prevented them from agglomeration after exposure to the magnetic field. Paramagnetic property is beneficial in preventing nanoparticles from forming large agglomerates, and dispersed nanoparticles could be cleared out from the human body quickly after the degradation of MagGel.[35] However, particle size characterized using SEM and ImageJ (15 ± 5 nm) was much smaller than that characterized using laser diffraction (77 ± 4 nm), mainly due to the difference between the two measuring methods. When measuring particle size based on the SEM image, boundaries of individual magnetic nanoparticle were outlined and quantified using ImageJ, thus representing the actual size of each nanoparticle. In contrast, the magnetic nanoparticles formed agglomerates in DI water when they were injected into the laser diffraction particle analyzer, even though high power sonication was used to disperse these nanoparticles. On the basis of the principles of laser diffraction, individual magnetic nanoparticle versus particle agglomerates could not be distinguished, and thus, both contributed to the overall particle size measurement. In other words, the larger particle size measured using laser diffraction was due to the presence of agglomerates.

EDS analysis (Figure 2B) showed the presence of Fe, Cl, O, and C in magnetic nanoparticles, which is expected from the source materials. During the synthesis, iron chloride reacted with ammonium hydroxide to form iron oxides ($FeO{\cdot}Fe_2O_3$). Specifically, Fe and Cl were from $FeCl_3$ and $FeCl_2{\cdot}4H_2O$, indicating a small amount of Cl (1 at. %) remained after the magnetic nanoparticles were washed with DI water for three times. PVA was also a possible source of the observed O peak, and it contributed to the C peak as well. EDS results showed the atomic ratio of Fe/O is 0.49, which was lower than the theoretical atomic ratio of 0.75 in Fe_3O_4. However, since EDS analysis could not differentiate the O signals from PVA or iron oxide, it is necessary to confirm the phase of the nanoparticles using XRD.

The XRD pattern of synthesized magnetic nanoparticles (Figure 2E) showed the presence of major peaks for Fe_3O_4, but absence of minor peaks for γ-Fe_2O_3, when compared with the standard XRD pattern of Fe_3O_4 and γ-Fe_2O_3, respectively. Combined with EDS analysis, we concluded that the nanoparticles were mostly in the form of magnetite Fe_3O_4. It is still possible that these nanoparticles were partially oxidized to the form of γ-Fe_2O_3 considering their brown color appearing in DI water (Figure 7B). However, the presence of γ-Fe_2O_3 crystals did not have any substantial influence on the cytocompatibility of these magnetic nanoparticles with BMSCs within 24 h based on our *in vitro* results. Moreover, γ-Fe_2O_3 was found to be cytocompatible with murine L929 fibroblasts,[36] human umbilical vein endothelial cells,[37] and HeLa cells.[38]

4.2. Characterization of the MagGel and Gel. To synthesize the gels, we extracted Col II from sheep stifle joint. Prior to extraction, the stifle joint was characterized using SEM and we observed a clear transition from hyaline cartilage to mineralized subchondral bone (Figure 3). FTIR analysis of the extracted type II condyle and tibia collagen showed the presence of amide A, I, II, and III groups (Figure 4), which is

DOI: 10.1021/acsami.5b06939
ACS Appl. Mater. Interfaces 2015, 7, 20987−20998

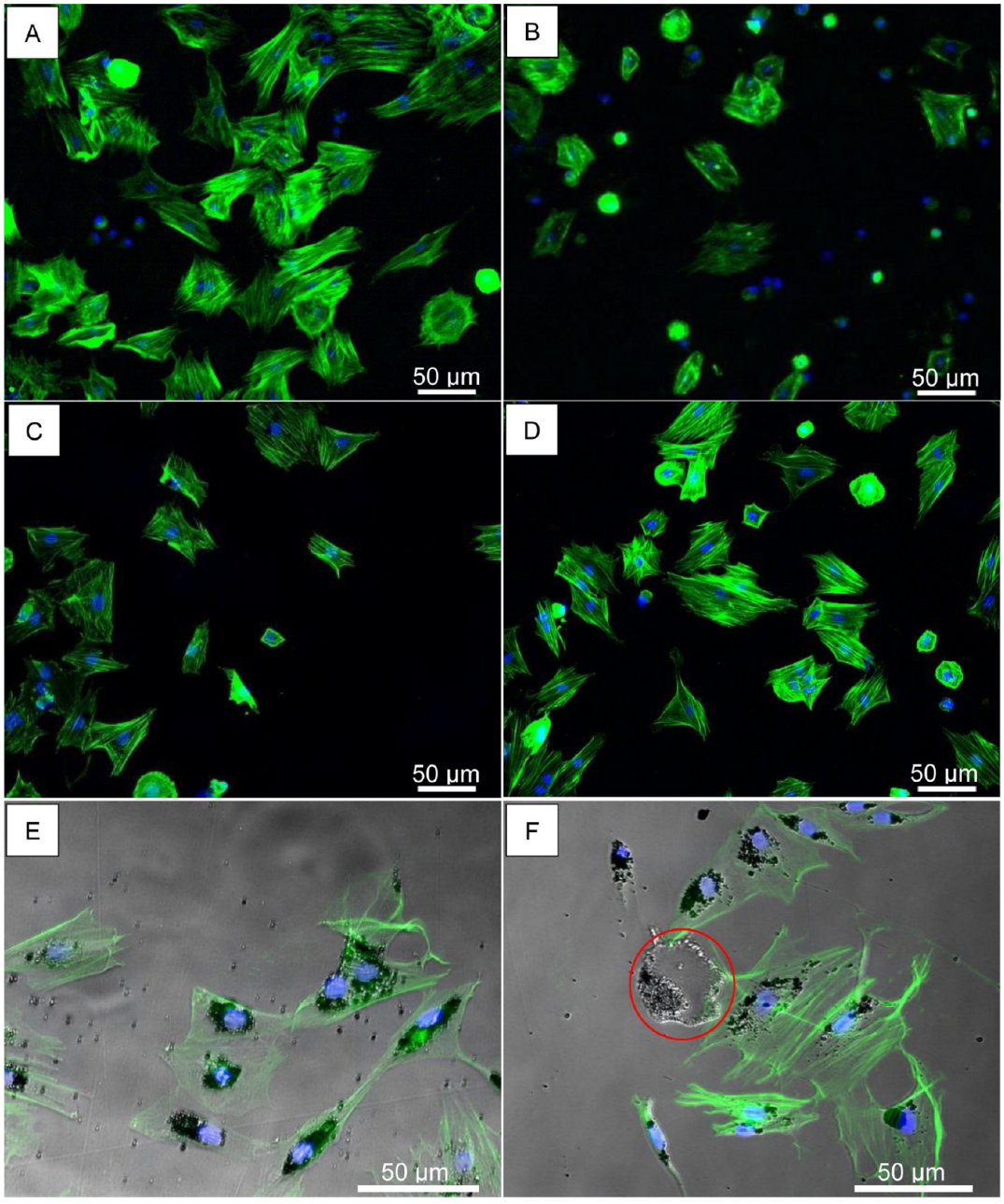

Figure 9. Fluorescence images of BMSC adhesion and morphology when cultured with materials of interest. (A) MagGel; (B) Gel; (C) magnetic nanoparticles on glass slides; (D) glass reference. (E, F) Fluorescence image overlay with bright field image, showing endocytosis of magnetic nanoparticles by BMSCs. Magnetic nanoparticles (black) intake by BMSCs did not enter the nucleus (stained in blue). F-actin of the BMSCs is stained in green. Red circle highlights the magnetic nanoparticles outside of the BMSCs. Scale bar = 50 μm.

consistent with the results reported by Barnes et al.[27] and other research groups.[39−41] FTIR spectra of the gels showed the conservation of amide A, I, II, and III bands of collagen as well as the C−H and C−N band of HA and 4-arm-PEG, respectively (Figure 5). The broad peak centered at 3300 cm^{-1} in both gels may also indicate the conservation of O−H stretching and N−H stretching vibrations in HA and 4-arm-PEG, respectively. The presence of C−O−C stretching at 945.8 and 842.7 cm^{-1} indicated the cross-linking of type II collagen with the 4-arm-PEG. The peaks of C−O−C are more apparent in the FTIR spectrum of MagGel than in the Gel. This might be caused by the presence of Fe. In another study, Abedini et al.[42] synthesized colloidal magnetite nanoparticles using γ radiation in an aqueous solution containing iron chloride in the presence of PVA. They also observed the presence of the small peak around 1100 cm^{-1} and attributed it to the presence of Fe ions.

In EDS analysis of the gels, the large amount of C and O and small amount of N were due to incorporation of Col II, HA, and PEG and the small amount of Fe in MagGel was from magnetic nanoparticles (Figure 6C,F). The incorporation of iron oxide did not affect the percentage of O but decreased the percentage of C and N in MagGel in a small range as compared with the Gel. The interaction of magnetic nanoparticles with other hydrogel components also increased the MagGel surface roughness compared to the Gel. Change of surface roughness through the addition of magnetic nanoparticles can also be seen in other studies.[43] In the SEM micrographs, circular-shaped

DOI: 10.1021/acsami.5b06939
ACS Appl. Mater. Interfaces 2015, 7, 20987−20998

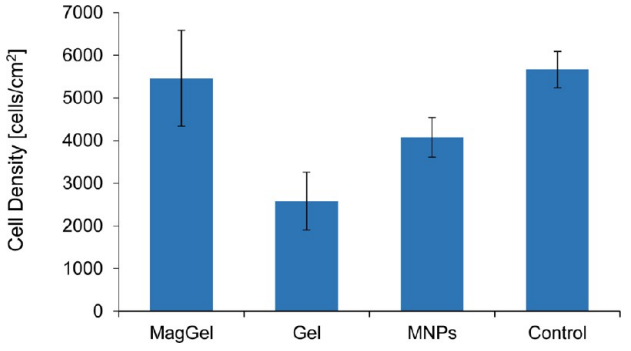

Figure 10. Cell density in each experimental group after 24 h of culture. From left to right: BMSCs cultured with MagGel, Gel, magnetic nanoparticles (MNPs), and control group (i.e., glass reference). Values are mean ± standard error. $p = 0.0563$ for ANOVA.

dark areas were observed on the surface of both gels (Figure 6A,D). Both SEM visual observation and EDS analysis showed that the darker areas had similar features and composition as other areas (data not shown). This artifact might have been induced by the lyophilization process during which the water droplets were extracted from the gel matrix. Interestingly, the surface features on the lyophilized gels were similar to those surface features observed in the cartilage−bone transition area.

The degradation of MagGel and Gel was individually studied in rSBF and PBS and also monitored during *in vitro* culture with BMSCs in DMEM. After 24 h of culture in DMEM with BMSCs, both MagGel and Gel completely disintegrated and could not be collected from the culture. The faster gel degradation in DMEM with cells was likely due to the presence of excreted enzymes that could reduce the gel cross-linking and accelerate gel degradation.

4.3. Characterization of BMSCs Adhesion and Morphology. The *in vitro* cell study showed that MagGel group had the greatest cell adhesion density on average when compared with the Gel group and magnetic nanoparticles group and a similar cell adhesion density as compared with the control, indicating good cytocompatibility within 24 h of culture. The ANOVA showed no statistically significant difference among all groups ($p = 0.0563 > 0.05$), but the p value was only slightly higher than the 0.05 significance level. It is possible that statistical significance might be detected with more repeats. Our hypothesis is that the synergistic effect of the hybrid gel and magnetic nanoparticles improved BMSC adhesion. First of all, the hybrid gel mimicked cartilage ECM, which provided a favorable environment for cells. Second, the interaction of magnetic nanoparticles with BMSCs might be beneficial for cell adhesion. Huang et al. demonstrated that the Fe_3O_4 nanoparticles increased human mesenchymal stem cells growth due to their ability to reduce intracellular H_2O_2 through intrinsic peroxidase-like activity. They also suggested that Fe_3O_4 nanoparticles could accelerate cell cycle progression.[44] Each magnetic nanoparticle could be considered as a small magnetic domain with a tiny magnetic field. When the magnetic nanoparticles are incorporated into the scaffold in a large number, the microenvironments inside or on the surface of the composite scaffold are composed of many tiny magnetic fields, and the total effect would likely be strengthened. As a result, the strengthened effect might affect ion channels on the cell membrane and initiate changes in cytoskeletal architecture under the magnetic field.[45,46] For a time period shorter than 24 h, we expect that the cell adhesion would be similar to the 24 h culture result since the cells usually adhere to a substrate 4 h after seeding and slowly adapt to the environment afterward. After 24 h, cells become more active in proliferation and migration. Besides, BMSCs have the potential to differentiate into chondrocytes, which would benefit the application of the hydrogels in cartilage tissue engineering. However, future research with a longer cell culture period is necessary to determine the long-term cytocompatibility of MagGel with BMSCs, proliferation and differentiation of BMSCs after 24 h, and the interaction mechanisms of MagGel with BMSCs.

Magnetic nanoparticle uptake by BMSCs was observed in cell culture. BMSCs maintained normal morphology with the magnetic nanoparticles in cytoplasm. Zhang et al.[47] reported that superparamagnetic magnetite nanoparticles (Fe_3O_4) could be uptaken by mouse macrophage cells RAW 264.7 and breast cancer cells. Wilhelm et al.[48] showed that maghemite (γ-Fe_2O_3) exhibited a high level of cellular internalization by mouse macrophages, which was mediated by the affinity with cell membrane and endocytosis. Since Fe_3O_4 and γ-Fe_2O_3 maghemite are very similar in structure and properties, we hypothesize that our synthesized magnetic nanoparticles were endocytosed as well. Besides, all the particles inside cells were distributed in cytoplasm but not in the nucleus, suggesting that either particle sizes were larger than the channel diameter of nuclear pore complexes (NPC)[49] or the control mechanism of NPC prevented the penetration of magnetic nanoparticles to protect cell genome.[50] The fact that the cell nuclei were particle-free might be the reason for the similar cell density when cultured with magnetic nanoparticles as compared with the control, indicating good cytocompatibility within 24 h of culture despite the particle uptake by BMSCs. It is possible that the ingested magnetic nanoparticles would be broken down by lysosome and expelled from the cells through exocytosis.[51] However, further research is needed to determine the exocytosis process.

It has been reported that a low frequency electromagnetic field could enhance chondrogenesis in human adipose-derived stem cells[52] and in human mesenchymal stem cells.[13] Thus, it is hypothesized that integration of electromagnetic field with the MagGel could further control cell functions, e.g., directing adhesion, proliferation, and differentiation of BMSCs. The combined effects of external magnetic field and MagGel on cell functions should be further studied for potential cartilage tissue regeneration.

5. CONCLUSIONS

The MagGel synthesized in this study provides a promising scaffold for potential cartilage tissue engineering because the MagGel responded to an external magnetic field, which could be used to direct the scaffold to the exact cartilage defect site remotely using an external magnet. Moreover, the MagGel showed similar microstructure and chemistry as hyaline cartilage and was cytocompatible with BMSCs *in vitro*, as demonstrated by the increased BMSC viability when compared with the Gel in the 24 h culture. However, further cell studies with these gels in the presence of an external magnet are still needed to determine the combined effects of magnetic field and magnetic scaffold on cell functions. In addition, the presence of magnetic nanoparticles did not affect the viability of BMSCs within 24 h of culture when compared with the control group. Although the hydrogels degraded much faster in DMEM with BMSCs than in rSBF or in PBS, further cross-linking of the gels

DOI: 10.1021/acsami.5b06939
ACS Appl. Mater. Interfaces 2015, 7, 20987−20998

could reduce the degradation rate of the hydrogels and improve the scaffold integrity for a longer period.

■ ASSOCIATED CONTENT

Supporting Information

The Supporting Information is available free of charge on the ACS Publications website at DOI: 10.1021/acsami.5b06939.

Supplemental video 1 showing the movement of MagGel in response to an external magnet (AVI)

Supplemental video 2 showing the movement of magnetic nanoparticles in response to an external magnet (AVI)

■ AUTHOR INFORMATION

Corresponding Author

*Phone: 951 827 2944. Fax: 951 827 6416. E-mail: huinan.liu@ucr.edu.

Notes

Any opinions, findings, and conclusions or recommendations expressed in this material are those of the author(s) and do not necessarily reflect the views of the National Science Foundation.

The authors declare no competing financial interest.

■ ACKNOWLEDGMENTS

The authors thank Hellman Faculty Fellowship (H.L.) and the University of California Regents Faculty Fellowship (H.L.) for financial support. The authors thank U.S. National Science Foundation Graduate Research Fellowship Program for supporting the graduate student researcher (GRFP 2012125281 for J.L.) and California Institute for Regenerative Medicine (CIRM) Bridges to Stem Cell Research for supporting the undergraduate student researcher (A.S.). The authors thank Central Facility for Advanced Microscopy and Microanalysis (CFAMM) at the University of California, Riverside, for the use of SEM and EDS and Dr. Krassimir Bozhilov for SEM/EDS training. The authors thank Dr. Lawrence D. Longo (NIH Grant HD031226) at Loma Linda University for providing sheep stifle joints for Type II collagen extraction. The authors thank Dr. Gary Botimer at Loma Linda University for the kind gift of Arithrex Osteochondral Autograft Transfer System (OATS) for harvesting the subchondral bone plugs.

■ REFERENCES

(1) Dai, W.; Kawazoe, N.; Lin, X.; Dong, J.; Chen, G. The Influence of Structural Design of PLGA/Collagen Hybrid Scaffolds in Cartilage Tissue Engineering. *Biomaterials* **2010**, *31*, 2141−2152.

(2) Tan, H.; Chu, C. R.; Payne, K. A.; Marra, K. G. Injectable in Situ Forming Biodegradable Chitosan−Hyaluronic Acid Based Hydrogels for Cartilage Tissue Engineering. *Biomaterials* **2009**, *30*, 2499−2506.

(3) Li, W.-J.; Tuli, R.; Huang, X.; Laquerriere, P.; Tuan, R. S. Multilineage Differentiation of Human Mesenchymal Stem Cells in a Three-Dimensional Nanofibrous Scaffold. *Biomaterials* **2005**, *26*, 5158−5166.

(4) Balasundaram, G.; Storey, D. M.; Webster, T. J. Novel Nano-Rough Polymers for Cartilage Tissue Engineering. *Int. J. Nanomed.* **2014**, *9*, 1845−1853.

(5) Park, G. E.; Pattison, M. A.; Park, K.; Webster, T. J. Accelerated Chondrocyte Functions on Naoh-Treated PLGA Scaffolds. *Biomaterials* **2005**, *26*, 3075−3082.

(6) Corr, S. A.; Byrne, S. J.; Tekoriute, R.; Meledandri, C. J.; Brougham, D. F.; Lynch, M.; Kerskens, C.; O'Dwyer, L.; Gun'ko, Y. K. Linear Assemblies of Magnetic Nanoparticles as MRI Contrast Agents. *J. Am. Chem. Soc.* **2008**, *130*, 4214−4215.

(7) Jain, T. K.; Richey, J.; Strand, M.; Leslie-Pelecky, D. L.; Flask, C. A.; Labhasetwar, V. Magnetic Nanoparticles with Dual Functional Properties: Drug Delivery and Magnetic Resonance Imaging. *Biomaterials* **2008**, *29*, 4012−4021.

(8) Lee, J.-H.; Jang, J.-t.; Choi, J.-s.; Moon, S. H.; Noh, S.-h.; Kim, J.-w.; Kim, J.-G.; Kim, I.-S.; Park, K. I.; Cheon, J. Exchange-Coupled Magnetic Nanoparticles for Efficient Heat Induction. *Nat. Nanotechnol.* **2011**, *6*, 418−422.

(9) Meenach, S. A.; Anderson, A. A.; Suthar, M.; Anderson, K. W.; Hilt, J. Z. Biocompatibility Analysis of Magnetic Hydrogel Nanocomposites Based on Poly(N-Isopropylacrylamide) and Iron Oxide. *J. Biomed. Mater. Res., Part A* **2009**, *91A*, 903−909.

(10) Bock, N.; Riminucci, A.; Dionigi, C.; Russo, A.; Tampieri, A.; Landi, E.; Goranov, V. A.; Marcacci, M.; Dediu, V. A Novel Route in Bone Tissue Engineering: Magnetic Biomimetic Scaffolds. *Acta Biomater.* **2010**, *6*, 786−796.

(11) Zhang, J.; Zhao, S.; Zhu, M.; Zhu, Y.; Zhang, Y.; Liu, Z.; Zhang, C. 3D-Printed Magnetic Fe_3O_4 /MBG/PCL Composite Scaffolds with Multifunctionality of Bone Regeneration, Local Anticancer Drug Delivery and Hyperthermia. *J. Mater. Chem. B* **2014**, *2*, 7583−7595.

(12) Kobayashi, T.; Ochi, M.; Yanada, S.; Ishikawa, M.; Adachi, N.; Deie, M.; Arihiro, K. Augmentation of Degenerated Human Cartilage in Vitro Using Magnetically Labeled Mesenchymal Stem Cells and an External Magnetic Device. *Arthroscopy* **2009**, *25*, 1435−1441.

(13) Mayer-Wagner, S.; Passberger, A.; Sievers, B.; Aigner, J.; Summer, B.; Schiergens, T. S.; Jansson, V.; Muller, P. E. Effects of Low Frequency Electromagnetic Fields on the Chondrogenic Differentiation of Human Mesenchymal Stem Cells. *Bioelectromagnetics* **2011**, *32*, 283−90.

(14) Nordin, M.; Frankel, V. I. *Basic Biomechanics of the Musculoskeletal System*, 3rd ed.; Lippincott Williams & Wilkins: Philadelphia, 2001.

(15) Unterman, S. A.; Gibson, M.; Lee, J. H.; Crist, J.; Chansakul, T.; Yang, E. C.; Elisseeff, J. H. Hyaluronic Acid-Binding Scaffold for Articular Cartilage Repair. *Tissue Eng., Part A* **2012**, *18*, 2497−2506.

(16) Levett, P. A.; Hutmacher, D. W.; Malda, J.; Klein, T. J. Hyaluronic Acid Enhances the Mechanical Properties of Tissue-Engineered Cartilage Constructs. *PLoS One* **2014**, *9*, e113216.

(17) Chow, G.; Knudson, C. B.; Homandberg, G.; Knudson, W. Increased Expression of Cd44 in Bovine Articular Chondrocytes by Catabolic Cellular Mediators. *J. Biol. Chem.* **1995**, *270*, 27734−27741.

(18) Aigner, J.; Tegeler, J.; Hutzler, P.; Campoccia, D.; Pavesio, A.; Hammer, C.; Kastenbauer, E.; Naumann, A. Cartilage Tissue Engineering with Novel Nonwoven Structured Biomaterial Based on Hyaluronic Acid Benzyl Ester. *J. Biomed. Mater. Res.* **1998**, *42*, 172−181.

(19) Yoo, H. S.; Lee, E. A.; Yoon, J. J.; Park, T. G. Hyaluronic Acid Modified Biodegradable Scaffolds for Cartilage Tissue Engineering. *Biomaterials* **2005**, *26*, 1925−1933.

(20) Bryant, S. J.; Anseth, K. S. Controlling the Spatial Distribution of ECM Components in Degradable Peg Hydrogels for Tissue Engineering Cartilage. *J. Biomed. Mater. Res.* **2003**, *64A*, 70−79.

(21) Jin, R.; Moreira Teixeira, L. S.; Krouwels, A.; Dijkstra, P.; Van Blitterswijk, C.; Karperien, M.; Feijen, J. Synthesis and Characterization of Hyaluronic Acid−Poly (Ethylene Glycol) Hydrogels Via Michael Addition: An Injectable Biomaterial for Cartilage Repair. *Acta Biomater.* **2010**, *6*, 1968−1977.

(22) Nguyen, K. T.; West, J. L. Photopolymerizable Hydrogels for Tissue Engineering Applications. *Biomaterials* **2002**, *23*, 4307−4314.

(23) Zhu, J. Bioactive Modification of Poly (Ethylene Glycol) Hydrogels for Tissue Engineering. *Biomaterials* **2010**, *31*, 4639−4656.

(24) Pfister, P. M.; Wendlandt, M.; Neuenschwander, P.; Suter, U. W. Surface-Textured PEG-Based Hydrogels with Adjustable Elasticity: Synthesis and Characterization. *Biomaterials* **2007**, *28*, 567−575.

(25) Hutson, C. B.; Nichol, J. W.; Aubin, H.; Bae, H.; Yamanlar, S.; Al-Haque, S.; Koshy, S. T.; Khademhosseini, A. Synthesis and Characterization of Tunable Poly(Ethylene Glycol): Gelatin Meth-

DOI: 10.1021/acsami.5b06939
ACS Appl. Mater. Interfaces 2015, 7, 20987−20998

acrylate Composite Hydrogels. *Tissue Eng., Part A* **2011**, *17*, 1713−1723.
(26) Zhou, L.; He, B.; Zhang, F. Facile One-Pot Synthesis of Iron Oxide Nanoparticles Cross-Linked Magnetic Poly (Vinyl Alcohol) Gel Beads for Drug Delivery. *ACS Appl. Mater. Interfaces* **2012**, *4*, 192−199.
(27) Barnes, C. P.; Pemble, C. W., IV; Brand, D. D.; Simpson, D. G.; Bowlin, G. L. Cross-Linking Electrospun Type II Collagen Tissue Engineering Scaffolds with Carbodiimide in Ethanol. *Tissue Eng.* **2007**, *13*, 1593−1605.
(28) Calderon, L.; Collin, E.; Murphy, M.; O'Halloran, D.; Pandit, A. Type II Collagen-Hyaluronan Hydrogel-a Step Towards a Scaffold for Intervertebral Disc Tissue Engineering. *Eur. Cells Mater.* **2010**, *20*, 134−148.
(29) Cipriano, A. F.; De Howitt, N.; Gott, S. C.; Miller, C.; Rao, M. P.; Liu, H. Bone Marrow Stromal Cell Adhesion and Morphology on Micro-and Sub-Micropatterned Titanium. *J. Biomed. Nanotechnol.* **2014**, *10*, 660−668.
(30) Thi-Hiep, N.; Van Hoa, D.; Van Toi, V. Injectable in Situ Crosslinkable Hyaluronan-Polyvinyl Phosphonic Acid Hydrogels for Bone Engineering. *J. Biomed. Sci. Eng.* **2013**, *6*, 854−862.
(31) Lu, C.; Zahedi, P.; Forman, A.; Allen, C. Multi-Arm PEG/Silica Hydrogel for Sustained Ocular Drug Delivery. *J. Pharm. Sci.* **2014**, *103*, 216−226.
(32) Elahi, M. F.; Guan, G.; Wang, L.; King, M. W. Influence of Layer-by-Layer Polyelectrolyte Deposition and EDC/NHS Activated Heparin Immobilization onto Silk Fibroin Fabric. *Materials* **2014**, *7*, 2956−2977.
(33) Xing, Q.; Yates, K.; Vogt, C.; Qian, Z.; Frost, M. C.; Zhao, F. Increasing Mechanical Strength of Gelatin Hydrogels by Divalent Metal Ion Removal. *Sci. Rep.* **2014**, *4*, 4706.
(34) Kilian, K. A.; Böcking, T.; Gaus, K.; Gooding, J. J. Introducing Distinctly Different Chemical Functionalities onto the Internal and External Surfaces of Mesoporous Materials. *Angew. Chem., Int. Ed.* **2008**, *47*, 2697−2699.
(35) Corchero, J. L.; Villaverde, A. Biomedical Applications of Distally Controlled Magnetic Nanoparticles. *Trends Biotechnol.* **2009**, *27*, 468−476.
(36) Luengo, Y.; Nardecchia, S.; Morales, M. P.; Serrano, M. C. Different Cell Responses Induced by Exposure to Maghemite Nanoparticles. *Nanoscale* **2013**, *5*, 11428−11437.
(37) Bakandritsos, A.; Mattheolabakis, G.; Zboril, R.; Bouropoulos, N.; Tucek, J.; Fatouros, D. G.; Avgoustakis, K. Preparation, Stability and Cytocompatibility of Magnetic/PLA-PEG Hybrids. *Nanoscale* **2010**, *2*, 564−572.
(38) Ereath Beeran, A.; Fernandez, F. B.; John, A.; Varma PR, H. Self-Assembled Superparamagnetic Nanocomposite-Labelled Cells for Noninvasive, Controlled, Targeted Delivery and Therapy. *RSC Adv.* **2015**, *5*, 36742−36752.
(39) Costantini, F.; Nascetti, A.; Scipinotti, R.; Domenici, F.; Sennato, S.; Gazza, L.; Bordi, F.; Pogna, N.; Manetti, C.; Caputo, D.; de Cesare, G. On-Chip Detection of Multiple Serum Antibodies against Epitopes of Celiac Disease by an Array of Amorphous Silicon Sensors. *RSC Adv.* **2014**, *4*, 2073−2080.
(40) Usha, R.; Sreeram, K.; Rajaram, A. Stabilization of Collagen with EDC/NHS in the Presence of L-Lysine: A Comprehensive Study. *Colloids Surf., B* **2012**, *90*, 83−90.
(41) Sam, S.; Touahir, L.; Salvador Andresa, J.; Allongue, P.; Chazalviel, J.-N.; Gouget-Laemmel, A.; Henry de Villeneuve, C.; Moraillon, A.; Ozanam, F.; Gabouze, N.; Djebbar, S. Semiquantitative Study of the EDC/NHS Activation of Acid Terminal Groups at Modified Porous Silicon Surfaces. *Langmuir* **2010**, *26*, 809−814.
(42) Abedini, A.; Daud, A. R.; Hamid, M. A. A.; Othman, N. K. Radiolytic Formation of Fe_3O_4 Nanoparticles: Influence of Radiation Dose on Structure and Magnetic Properties. *PLoS One* **2014**, *9*, e90055.
(43) Gloria, A.; Russo, T.; D'Amora, U.; Zeppetelli, S.; D'Alessandro, T.; Sandri, M.; Bañobre-López, M.; Piñeiro-Redondo, Y.; Uhlarz, M.; Tampieri, A.; Rivas, J.; Herrmannsdörfer, T.; Dediu, V. A.; Ambrosio, L.; De Santis, R. Magnetic Poly(E-Caprolactone)/Iron-Doped Hydroxyapatite Nanocomposite Substrates for Advanced Bone Tissue Engineering. *J. R. Soc., Interface* **2013**, *10*, 1−11.
(44) Huang, D.-M.; Hsiao, J.-K.; Chen, Y.-C.; Chien, L.-Y.; Yao, M.; Chen, Y.-K.; Ko, B.-S.; Hsu, S.-C.; Tai, L.-A.; Cheng, H.-Y.; et al. The Promotion of Human Mesenchymal Stem Cell Proliferation by Superparamagnetic Iron Oxide Nanoparticles. *Biomaterials* **2009**, *30*, 3645−3651.
(45) Hughes, S.; El Haj, A. J.; Dobson, J. Magnetic Micro-and Nanoparticle Mediated Activation of Mechanosensitive Ion Channels. *Med. Eng. Phys.* **2005**, *27*, 754−762.
(46) Shen, J.-F.; Chao, Y.-L.; Du, L. Effects of Static Magnetic Fields on the Voltage-Gated Potassium Channel Currents in Trigeminal Root Ganglion Neurons. *Neurosci. Lett.* **2007**, *415*, 164−168.
(47) Zhang, Y.; Kohler, N.; Zhang, M. Surface Modification of Superparamagnetic Magnetite Nanoparticles and Their Intracellular Uptake. *Biomaterials* **2002**, *23*, 1553−1561.
(48) Wilhelm, C.; Gazeau, F.; Roger, J.; Pons, J.; Bacri, J.-C. Interaction of Anionic Superparamagnetic Nanoparticles with Cells: Kinetic Analyses of Membrane Adsorption and Subsequent Internalization. *Langmuir* **2002**, *18*, 8148−8155.
(49) Mohr, D.; Frey, S.; Fischer, T.; Güttler, T.; Görlich, D. Characterisation of the Passive Permeability Barrier of Nuclear Pore Complexes. *EMBO J.* **2009**, *28*, 2541−2553.
(50) Jamali, T.; Jamali, Y.; Mehrbod, M.; Mofrad, M. Nuclear Pore Complex: Biochemistry and Biophysics of Nucleocytoplasmic Transport in Health and Disease. *Int. Rev. Cell Mol. Biol.* **2011**, *287*, 233−286.
(51) Park, S.; Kim, H. S.; Kim, W. J.; Yoo, H. S. Pluronic@ Fe_3O_4 Nanoparticles with Robust Incorporation of Doxorubicin by Thermo-Responsiveness. *Int. J. Pharm.* **2012**, *424*, 107−114.
(52) Chen, C.-H.; Lin, Y.-S.; Fu, Y.-C.; Wang, C.-K.; Wu, S.-C.; Wang, G.-J.; Eswaramoorthy, R.; Wang, Y.-H.; Wang, C.-Z.; Wang, Y.-H.; et al. Electromagnetic Fields Enhance Chondrogenesis of Human Adipose-Derived Stem Cells in a Chondrogenic Microenvironment in Vitro. *J. Appl. Physiol.* **2013**, *114*, 647−655.

DOI: 10.1021/acsami.5b06939
ACS Appl. Mater. Interfaces 2015, 7, 20987−20998